

# Capacitive Micromachined Ultrasonic Transducers: Theory and Technology

Arif S. Ergun<sup>1</sup>; Goksen G. Yaralioglu<sup>2</sup>; and Butrus T. Khuri-Yakub<sup>3</sup>

**Abstract:** Capacitive micromachined ultrasonic transducers (CMUTs), introduced about a decade ago, have been shown to be a good alternative to conventional piezoelectric transducers in various aspects, such as sensitivity, transduction efficiency, and bandwidth. In this paper, we discuss the principles of capacitive transducer operation that underlie these aspects. Many of the key features of capacitive ultrasonic transducers are enabled with micromachining technology. Micromachining allows us to miniaturize device dimensions and produce capacitive transducers that perform comparably to their piezoelectric counterparts. The fabrication process is described briefly, and the performance of the CMUT transducers is evaluated by demonstrating characterization results. It is shown that the transduction efficiency as defined by the electromechanical coupling coefficient can be close to unity with proper device design and operating voltage. It is also shown that CMUTs provide large bandwidth (123% fractional bandwidth) in immersion applications which translate into high temporal and axial resolution. Finally, the feasibility of using CMUTs is demonstrated by showing imaging examples in air and in immersion.

**DOI:** 10.1061/(ASCE)0893-1321(2003)16:2(76)

**CE Database subject headings:** Transducers; Fabrication; Imaging techniques; Electronic equipment.

## Introduction

Electrostatic transducers have long been in use for sound wave excitation and detection (Kuhl 1954; Hunt 1982). The fundamental mechanism of the transduction is the vibration of a thin plate under electrostatic forces. Many macroscale devices use this mechanism for generating and sensing sonic waves. A condenser microphone is the most well-known example. In the simplest form of this device, a thin metal membrane is stretched above a back electrode forming a small gap. This structure constitutes a capacitor, which is charged by a dc voltage applied through a large resistor. When the device is exposed to sound waves, the gap height is modulated at the same frequency of the incoming pressure field. This induces a change in the device capacitance, generating an output voltage proportional to the amplitude of the field. The capacitor structure can also be used to generate sound waves. If the biased membrane is driven by an ac voltage, a harmonic field is generated in the sound-bearing medium.

The striking advantage of the electrostatic devices compared to the other types of transducers such as piezoelectric and magnetostrict is the inherent impedance match between the transducer and the surrounding medium. The low-mechanical impedance of the membrane is usually negligible. This results in very efficient

coupling of the sound waves into and from the sound-bearing medium.

Recent advances in the silicon micromachining techniques enabled the fabrication of microelectro-mechanical systems (MEMS) based electrostatic transducers (Haller and Khuri-Yakub 1996; Soh et al. 1996; Ladabaum et al. 1998). Miniaturization capability of the silicon micromachining process made the fabrication of devices working at ultrasonic frequencies possible. These devices are called capacitive micromachined ultrasonic transducers (CMUTs). CMUTs are made of small and thin membranes that are suspended over a conductive silicon substrate by insulating posts. The diameter of the membrane ranges from 10  $\mu\text{m}$  to hundreds of micrometers. The gap between the membrane and the substrate is vacuum sealed or left unsealed at will and it can be as small as 500  $\text{\AA}$ . The membranes are either conductive or coated with a conductive electrode and essentially create small capacitors together with the substrate. This structure results in very efficient transducers that can compete with their piezoelectric counterparts in terms of efficiency and bandwidth.

The small and thin membranes that constitute the CMUT transducer are micromachined onto a silicon substrate. Micromachining has evolved from the integrated circuit manufacturing technology as a means of fabricating microelectromechanical systems, and therefore has all the abilities that the integrated circuit technology has. These abilities include, but are not limited to, batch fabrication, and a high level of integration and scalability. Thus, with this technology, batch fabrication of high-density transducer arrays, as well as single elements are enabled. In addition, the scalability provides the ability to fabricate transducers with a wide range of size and shapes. Because the transducer response is primarily determined by the size and the shape of the membranes, scalability translates into the ability to fabricate a wide range of devices for operation at different frequency spans and regimes.

This paper summarizes the work that has been done on CMUTs. In the next section, the principle of operation and under-

<sup>1</sup>E. L. Ginzton Laboratory, Stanford Univ., Stanford, CA 94305-4088. E-mail: sanli@stanford.edu

<sup>2</sup>E. L. Ginzton Laboratory, Stanford Univ., Stanford, CA 94305-4088. E-mail: goksenin@stanford.edu

<sup>3</sup>E. L. Ginzton Laboratory, Stanford Univ., Stanford, CA 94305-4088. E-mail: khuri-yakub@stanford.edu

Note. Discussion open until September 1, 2003. Separate discussions must be submitted for individual papers. To extend the closing date by one month, a written request must be filed with the ASCE Managing Editor. The manuscript for this paper was submitted for review and possible publication on November 6, 2002; approved on November 6, 2002. This paper is part of the *Journal of Aerospace Engineering*, Vol. 16, No. 2, April 1, 2003. ©ASCE, ISSN 0893-1321/2003/2-76-84/\$18.00.

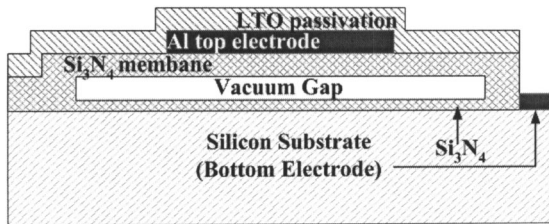


Fig. 1. Cross-sectional schematic drawing of membrane

lying theory are presented. In addition, the one-dimensional model that can be used to calculate basic device parameters such as capacitance, collapse voltage, and electromechanical coupling coefficient, will be discussed. In the section, "Fabrication Technology," the details of the fabrication principles and techniques will be described. The characterization procedures and their relevance to the device performance are discussed in the section, "Electrical and Acoustical Characterization." After the discussion on the applications of the CMUTs in the section, "Applications," conclusions are drawn.

## Principle of Operation

CMUTs are made of thin membranes which are essentially parallel plate capacitors with a gap between the plates. Fig. 1 is a schematic drawing of the cross section of a typical membrane. The conductive silicon wafer on which the membrane is fabricated make up one of the plates of the capacitor. The other plate of the capacitor is the metal electrode on top of the membrane. The membrane is supported with insulating posts. The membrane is generally made of an insulating material, most commonly silicon nitride ( $\text{Si}_3\text{N}_4$ ), and coated with a metal electrode. However, the membrane can be made of a conductive material in which case the metal top electrode is not necessary. Optionally, the top electrode can be coated with an insulating material such as low-temperature silicon dioxide (LTO) to provide electrical isolation from the surrounding medium.

CMUTs are used both as acoustic transmitters and receivers. On transmit, electrostatic attraction forces are used to put the membranes into vibration by applying an ac voltage. However, because electrostatic force is unipolar (always attraction), the vibration frequency of the membranes is twice of the applied frequency. Therefore, a dc bias voltage which is larger than the ac voltage amplitude is required for proper operation of CMUTs. The vibration of the membranes generates acoustical waves in the surrounding medium.

On receive mode, harmonic vibration of the membranes, caused by an incident acoustic wave, is detected using a capacitive detection, which also requires a dc voltage. The vibrations of the membranes cause a modulation on the overall device capacitance. Under the constant bias voltage supplied, the capacitance variations result in a current flow in the external electric circuit which is amplified for further processing. Fig. 2 shows the schematics of the electrical circuits used for generation and detection of acoustic waves with CMUTs.

## Collapse Voltage

As mentioned above, CMUTs require a dc bias voltage for proper operation. When a dc voltage is applied to the membrane, the electrostatic force pulls the membrane toward the substrate, which

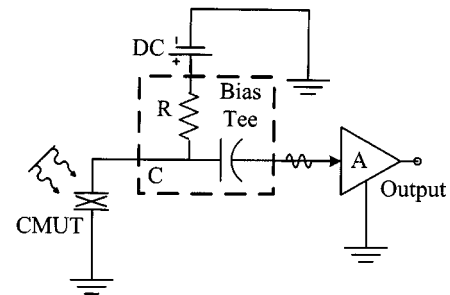
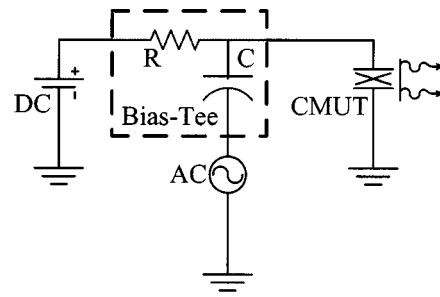


Fig. 2. Electrical circuits used to drive CMUTs in (a) transmit and (b) receive mode

is balanced by the mechanical restoring force of the membrane. As the bias voltage is increased, deflection of the membrane increases. However, above a certain voltage, called the collapse voltage, the electrostatic force overwhelms the restoring force and the membrane falls down on to the substrate. Therefore, the bias voltage should be kept less than this voltage. Yet, it should be close to the collapse voltage for maximum efficiency (Hunt 1982).

The collapse voltage can be calculated approximately by using a first-order model, which neglects the fringing electrostatic fields and the curvature of the membrane. Thus, the model consists of a spring whose constant is determined by the bending stiffness of the membrane and the electrostatic force acting on the spring. Assuming the membrane is moving like a piston, the total force exerted on the membrane is given by

$$F_{\text{elec}} = \frac{\epsilon_0 A V^2}{2(d_0 - x)^2} \quad (1)$$

where  $\epsilon_0$  = permittivity of free space;  $A$  = area;  $V$  = applied dc voltage;  $x$  = membrane displacement; and  $d_0$  = initial gap height. In the equilibrium position, this electrical force is balanced by the restoring force. Assuming  $k$  is the spring constant of the membrane, mechanical force exerted by the membrane is

$$F_{\text{mech}} = kx \quad (2)$$

By equating Eqs. (1) and (2), one finds the relation between the membrane displacement and applied dc voltage

$$V = \sqrt{\frac{2kx}{A\epsilon_0}} (d_0 - x) \quad (3)$$

The above equation can be arranged into a polynomial in  $x$ . For small bias voltages, this polynomial has only one real root smaller than the gap height. For voltages above the collapse voltage, the electrostatic force gradient is larger than the mechanical force gradient, and the polynomial equation does not give a physical solution. The displacement at the point of collapse can be found by equating  $dV/dx$  to zero, then, the collapse occurs at

$$x = \frac{d_0}{3} \quad (4)$$

and the collapse voltage is

$$V_{\text{coll}} = \sqrt{\frac{8kd_0^3}{27\epsilon_0 A}} \quad (5)$$

The above analysis assumes that the membrane is conducting and the electrostatic forces are applied to the bottom surface of the membrane. In actual devices, the membrane is usually made of a dielectric material and the electrodes are formed by depositing a metal on top of the membrane. In this case, the above analysis requires a simple modification. The effect of the membrane can be included by changing the gap height  $d_0$  with the effective gap height  $d_{\text{eff}}$ , which is given by

$$d_{\text{eff}} = \frac{d_m}{\epsilon_r} + d_0 \quad (6)$$

where  $d_m$  = membrane thickness and  $\epsilon_r$  = relative dielectric constant of the membrane material. In addition, the capacitance of the membrane is calculated using the following expression:

$$C(x) = \frac{A\epsilon_0}{d_{\text{eff}} - x} \quad (7)$$

As a final note, more accurate calculations can be carried out by using finite-element analysis to include the effect of membrane curvature and fringing fields (Bayram et al. 2001).

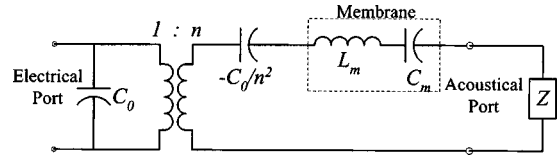


Fig. 3. Electrical equivalent circuit model of electromechanical transducer

### Electrical Equivalent Circuit Model

The analysis of CMUT transducers utilize the equivalent circuit model introduced by Mason for electroacoustic devices (Mason 1948). In the equivalent circuit shown in Fig. 3, the capacitor on the electrical side is the device capacitance of the CMUT element which is calculated in the previous subsection. The negative capacitance accounts for the spring softening effect due to the electromechanical interaction (Hunt 1982). The spring softening will be discussed later. On the acoustical side, the inductor and the capacitor represent the complex mechanical impedance of the CMUT, whereas the impedance  $Z$  is the acoustical impedance of the surrounding medium which is, in general, real. Finally, the transformer represents the electromechanical conversion between the electrical and the acoustical ports.

The mechanical impedance of the membrane is calculated by solving the fourth-order differential equation of motion on the membrane (Mason 1948)

$$Z_m = j\omega\rho d_m \frac{ak_1k_2[k_2J_0(k_1a)I_1(k_2a) + k_1J_1(k_1a)I_0(k_2a)]}{ak_1k_2[k_2J_0(k_1a)I_1(k_2a) + k_1J_1(k_1a)I_0(k_2a)] - 2(k_1^2 + k_2^2)J_1(k_1a)I_1(k_2a)} \quad (8)$$

where  $J_0$  and  $J_1$  = Bessel functions;  $I_0$  and  $I_1$  = modified Bessel functions;  $\omega$  = radian frequency; and  $\rho$  = density of the membrane material.  $k_1$  and  $k_2$  are given by the following equations:

$$k_1 = \sqrt{\frac{\sqrt{d^2 + 4c\omega^2} - d}{2c}}$$

$$k_2 = \sqrt{\frac{\sqrt{d^2 + 4c\omega^2} + d}{2c}} \quad (9)$$

$$c = \frac{(Y_0 + T)d_m^2}{12\rho(1 - \sigma^2)}$$

$$d = \frac{T}{\rho}$$

In these equations,  $Y_0$  = Young's modulus;  $T$  = residual stress; and  $\sigma$  = Poisson's ratio. The membrane impedance is purely imaginary and can be represented by a series inductance-capacitance circuit. If  $C_m$  and  $L_m$  represent the equivalent capacitance and inductance, respectively, the spring constant of the membrane is given by

$$k = \frac{1}{C_m} \quad (10)$$

One of the most important elements of the equivalent circuit is the transformer ratio which is derived as

$$n = V \frac{\epsilon_0 A}{(d_{\text{eff}} - x)^2} \quad (11)$$

In general, the sensitivity of a transducer is determined by the transformer ratio which is inversely proportional to the square of the cavity depth. One can achieve high-transformation ratios with CMUTs because surface micromachining allows us to make relatively small gaps (as low as 0.05  $\mu\text{m}$ ). Therefore, it is possible to achieve high-sensitivity values that are comparable to that of piezoelectric transducers.

### Electromechanical Coupling Coefficient

In general, transducers convert energy from one domain to another. For acoustic transducers, the conversion is between electrical and mechanical domains. The electromechanical coupling coefficient is defined as

$$k_T^2 = \frac{E_{\text{mech}}}{E_{\text{total}}} = \frac{1}{1 + \frac{E_{\text{elec}}}{E_{\text{mech}}}} \quad (12)$$

where  $E_{\text{mech}}$  = stored mechanical energy and  $E_{\text{elec}}$  = stored electrical energy.

One of the most important properties of an electrostatic trans-

ducer is that the small signal spring constant of the membrane is modified by the electromechanical interaction. This effect is called spring softening (Hunt 1982). The softened spring constant of the membrane vibrating in an electrostatic field is given by

$$k' = k(1 - k_T^2) \quad (13)$$

The above equation can also be used to determine the coupling coefficient by calculating the softened spring constant. However, we will use another approach for the calculation. For piezoelectric transducers, Belincourt defined free and fixed capacitances and calculated the coupling coefficient (Belincourt 1971). Later, Fraser adopted this method for CMUTs (Fraser and Reynolds 2000) and used finite-element analysis for the calculation of fixed and free capacitances.

The fixed capacitance is defined as the total capacitance of the transducer at a given dc bias

$$C^S = C(x)|_{x_{dc}, V_{dc}} \quad (14)$$

The free capacitance is defined as

$$C^T = \frac{dQ(x)}{dV} \Big|_{x_{dc}, V_{dc}} = \frac{d}{dV}(VC^S) \Big|_{x_{dc}, V_{dc}} \quad (15)$$

and the coupling coefficient is given by

$$k_T^2 = 1 - \frac{C^S}{C^T} \quad (16)$$

The fixed and free capacitances can be calculated using one-dimensional model presented in the section, "Collapse Voltage." The fixed capacitance is given by Eq. (7) repeated here for completeness

$$C^S = \frac{\epsilon_0 A}{d_{\text{eff}} - x} \quad (17)$$

and free capacitance is

$$C^T = \frac{\epsilon_0 A}{d_{\text{eff}} - x} + V \frac{\epsilon_0 A}{(d_{\text{eff}} - x)^2} \frac{dx}{dV} \quad (18)$$

If the derivative from Eq. (3) is substituted in the above equation free capacitance is obtained as

$$C^T = \frac{\epsilon_0 A}{d_{\text{eff}} - 3x} \quad (19)$$

and the coupling coefficient as

$$k_T^2 = \frac{2x}{d_{\text{eff}} - x} \quad (20)$$

The above result is important because at the collapse point ( $d_{\text{eff}}/3$ ), the coupling coefficient approaches unity, indicating that all the energy in one domain is converted to the other domain. Fig. 4 shows the electromechanical coupling coefficient as a function of bias voltage.

### Frequency Bandwidth

The main advantage of the equivalent circuit model of Fig. 3 is that it enables quick prediction of the response of the transducer in different media. A CMUT transducer is normally a resonant device and modeled with a resistor, inductor, and capacitor (RLC) circuit as shown in the mechanical port of the equivalent circuit model. The Q factor of this resonant structure is determined by the resistive load  $Z$  which represents the acoustical impedance of the medium. In air, because of the low-acoustical impedance, the

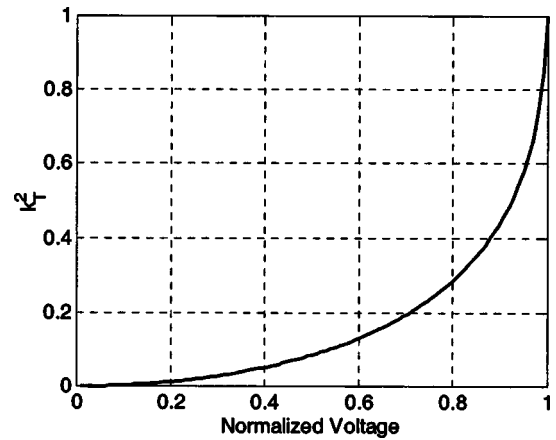


Fig. 4. Electromechanical coupling coefficient as function of voltage normalized to collapse voltage

Q factor of the resonant circuit is high, whereas in immersion the high acoustic impedance of water overdamps the resonant behavior. Another way to look at this is to compare the mechanical membrane impedance,  $j\omega L_m + 1/(j\omega C_m)$ , with the acoustical load  $Z$ . According to the model, the electrostatic force generated on the mechanical port is divided between the mechanical impedance of the membrane and the acoustical load, just like a voltage division. For frequencies where the mechanical impedance of the transducer (here the spring softening capacitance modeled as  $-C_0/n^2$  can be included in the total mechanical impedance) is small compared to the acoustical load, all of the electrostatic force generated on the mechanical port appears across the load. This frequency range primarily determines the frequency bandwidth of the transducer. Fig. 5 is a plot of the imaginary mechanical impedance of a CMUT element made of 28 membranes each with a  $36 \mu\text{m}$  diameter. The total size of the element is  $80 \mu\text{m}$  by  $560 \mu\text{m}$ . By comparing the mechanical impedance of this CMUT element to the acoustical impedance of water ( $1.5 \times 10^6 \text{ N s/m}^3$ ), one can predict the bandwidth of this particular CMUT. The plot in Fig. 5 suggests a 3-dB bandwidth between the frequencies 4 and 36 MHz, which corresponds to a fractional 3-dB bandwidth of 160%. Note that the impedance levels are normalized to area.

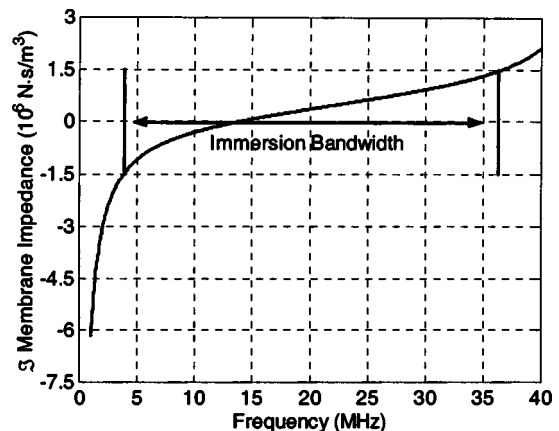
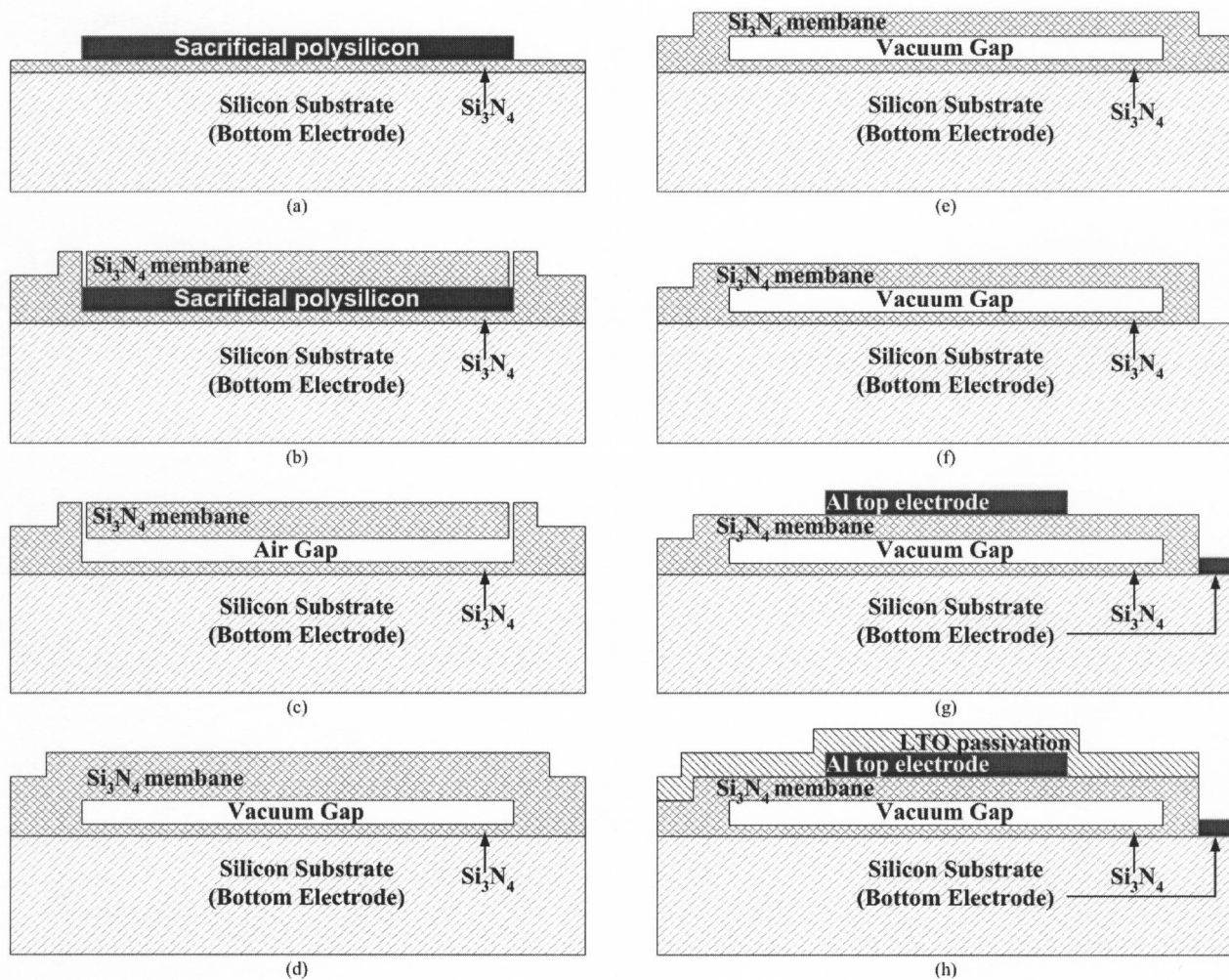


Fig. 5. Mechanical impedance of typical CMUT element designed for operation in 5–35 MHz range in immersion



**Fig. 6.** Simplified cross section of process flow for standard CMUT fabrication process: The silicon wafer is heavily doped and coated with etch stop layer of  $\text{Si}_3\text{N}_4$ . Then, (a) sacrificial polysilicon layer is deposited and patterned, (b) membrane  $\text{Si}_3\text{N}_4$  is deposited and etch holes are patterned through the membrane, (c) sacrificial polysilicon layer is selectively etched with KOH to release the  $\text{Si}_3\text{N}_4$  membrane, (d) small etch holes are sealed with an additional layer of  $\text{Si}_3\text{N}_4$  deposition, (e) membrane is etched back to its final thickness, (f) opening through the  $\text{Si}_3\text{N}_4$  layers provides electrical connection to bottom electrode, (g) aluminum is deposited and patterned which constitute top electrode and electrical connections, (h) and finally the aluminum electrodes are coated with thin layer of LTO to provide electrical isolation from surrounding.

## Fabrication Technology

In general, CMUTs are fabricated using surface micromachining technology, meaning all the processing is done on the surface of the silicon wafer by means of thin-film depositions, thin-film etching, and photolithography. But, it is also possible to integrate the CMUT process with bulk micromachining processes. Recently, CMUT fabrication that utilizes the wafer bonding technique has been demonstrated (Oralkan et al., unpublished, 2002). It has also been demonstrated that CMUTs can be integrated with electrical through-wafer interconnects, toward fabrication of two-dimensional (2D) CMUT arrays (Cheng et al. 2002). In this section, we will describe the standard CMUT fabrication process. Readers are encouraged to see relevant references for more information on the variations of this technology.

The CMUT fabrication process starts with a low-resistivity silicon wafer. The silicon wafer is heavily doped to achieve high conductivity at the surface which will become the bottom electrode of the CMUT later. Then, a thin ( $\sim 1,000 \text{ \AA}$ ) layer of liquid phase chemical vapor deposition (LPCVD)  $\text{Si}_3\text{N}_4$  (silicon nitride)

is deposited as an etch stop for the following sacrificial layer etching. Polycrystalline silicon (polysilicon) is deposited by LPCVD and patterned in order to form the sacrificial layer that defines the cavity [Fig. 6(a)]. A second layer of  $\text{Si}_3\text{N}_4$  is deposited with LPCVD that later forms the membrane. Several etch holes are dry etched into the silicon nitride membrane [Fig. 6(b)] to allow a path for the potassium hydroxide (KOH) to selectively etch the sacrificial polysilicon layer. At this step, the selectivity of the wet etch is important. The etchant should etch the sacrificial polysilicon as fast as possible without etching the  $\text{Si}_3\text{N}_4$  membrane significantly. Cold KOH etch provides the necessary selectivity between polysilicon and  $\text{Si}_3\text{N}_4$  ( $\sim 400,000:1$ ) to do the membrane release [Fig. 6(c)]. KOH etches silicon as well, which is avoided by the thin etch stop layer of  $\text{Si}_3\text{N}_4$  deposited at the beginning of the fabrication process. The size and thickness of the membrane and the gap have an important impact on the wet release process. Capillary forces acting on the membrane, while drying after the wet release, may collapse the membrane permanently to the substrate (Mastrangelo and Hsu 1993a,b). The size

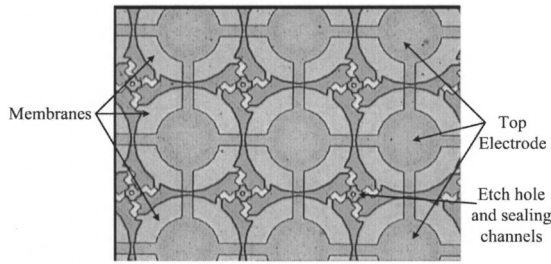


**Fig. 7.** Optical picture of actual device showing several membranes from top which are 100  $\mu\text{m}$  in diameter

and the thicknesses are designed and processed accordingly.

After the wet release of the membranes, the gap is sealed with a third layer of LPCVD  $\text{Si}_3\text{N}_4$  deposition which covers all the surfaces conformably; including the walls of the small etch holes. Therefore, a sufficient amount of  $\text{Si}_3\text{N}_4$  seals the etch holes. Because the deposition is done in low pressure ( $\sim 8$  Pa), the cavity is vacuum sealed [Fig. 6(d)]. The sealing process can be improved further by introducing some variations into the process (Jin et al. 1999). After the sealing step, the membrane has to be etched back to the final thickness [Fig. 6(e)]. Because the gap is vacuum sealed, the membrane deflects towards the substrate due to ambient pressure, which determines the final gap height. Therefore, the initial gap height as defined by the sacrificial polysilicon layer thickness, should be designed accordingly.

An opening through the  $\text{Si}_3\text{N}_4$  layers is etched to get access to the doped silicon substrate prior to metallization [Fig. 6(f)]. Aluminum is sputtered on the wafer and then patterned to define the

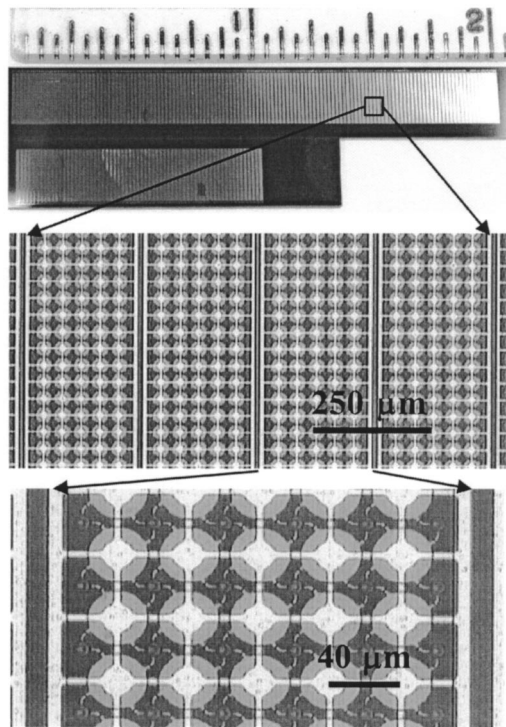


**Fig. 8.** Optical picture of 128 element 1D array (top), where each element, separated with 250  $\mu\text{m}$  pitch, is 200  $\mu\text{m}$  wide and 6 mm long (middle). Each array element consists of 600 membranes each with 36  $\mu\text{m}$  diameter (bottom).

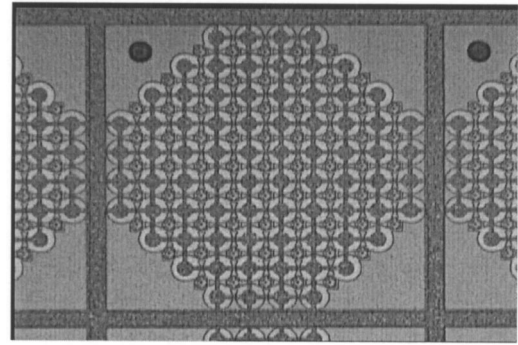


**Fig. 9.** Optical picture of 2D array element that is 400  $\mu\text{m}$  by 400  $\mu\text{m}$  in size and consists of 76 membranes which are 36  $\mu\text{m}$  in diameter. Block dot is electrical through wafer interconnect that brings electrical connection of each array element to backside of wafer.

top electrode of the membrane and the connection pads [Fig. 6(g)]. The final step is to cover the metal electrodes with an electrically insulating layer (LTO) and pattern it for wire bonding [Fig. 6(h)]. The wire bonds and pads are then covered with epoxy to ensure electrical passivation in conducting fluids, and to avoid corrosion.

Fig. 7 shows a magnified optical picture of a CMUT element. The membrane size for this particular device is 96  $\mu\text{m}$  in diameter. The top electrode covers approximately half of the membrane, and connects all the membranes electrically so the membranes move in unison. The etch hole is not located on the membrane, but connected to the membrane through channels. This structure results in a better sealing process as described in another publication (Jin et al. 1999). Fig. 8 is a picture of a CMUT array that consists of 128 elements. The element pitch is 250  $\mu\text{m}$  designed for imaging at 3 MHz. Each element is 20  $\mu\text{m}$  wide and 6 mm long, and consists of 600 membranes. Fig. 9 is a picture of a CMUT element, 400  $\mu\text{m}$  by 400  $\mu\text{m}$  in size, which is an element of a 128 by 128 2D CMUT array. The black dot on the picture is the electrical through-wafer interconnect that brings the electrical connection of each array element to the backside of the wafer.

### Electrical and Acoustical Characterization

The required dc bias is applied to the CMUT through a bias tee which essentially adds the dc and the ac voltages as previously shown in Fig. 2. In all the characterizations that will be discussed here, a similar biasing circuitry is used.

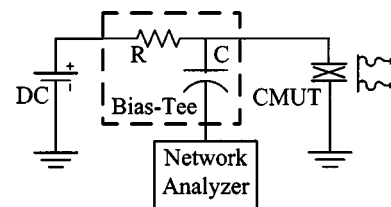


**Fig. 10.** Schematic of experimental setup used for input impedance measurements

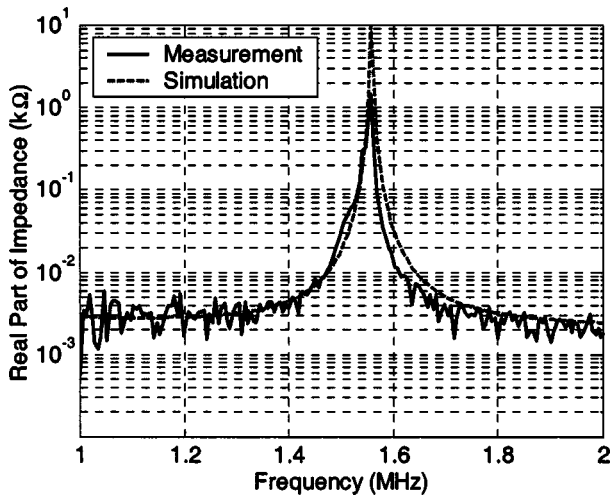


Fig. 11. Electrical input impedance measurement in air in comparison with simulation result: Real part

### Electrical Input Impedance Measurements

The electrical input impedance measurements provide a first proxy of the acoustical activity of the transducer. The measurements were performed with a vector network analyzer (HP 8751A) that measured the complex input impedance of the transducer as a function of frequency. The measurement setup is shown in Fig. 10. The network analyzer applies a small ac signal to measure the input impedance of the CMUT while sweeping the frequency.

The electrical input impedance measurements, primarily, allow us to validate the electrical equivalent circuit (Fig. 3) that is used to model the CMUT operation. The input impedance of the model can be calculated and compared to the measurement results. It is also possible to extract values for the components of the electrical equivalent model from the impedance data by utilizing a curve-fitting algorithm. The measurements can be carried out in vacuum, in air, and in water to validate the model further for different acoustical loads. Fig. 11 shows the real part of the electrical input impedance of a CMUT transducer in comparison with the simulation result. This particular CMUT is made of 4,900 membranes each with 96  $\mu\text{m}$  diameter. The total size of the device is 7 mm  $\times$  7 mm. The resonant behavior in the real part of the impedance curve revealed an acoustical activity. By comparing the simulation result to the actual measurement result we were

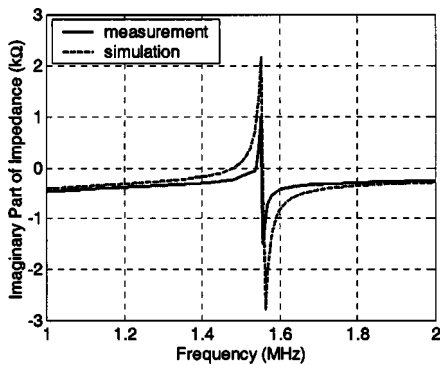


Fig. 12. Electrical input impedance measurement in air in comparison with simulation results: Imaginary part

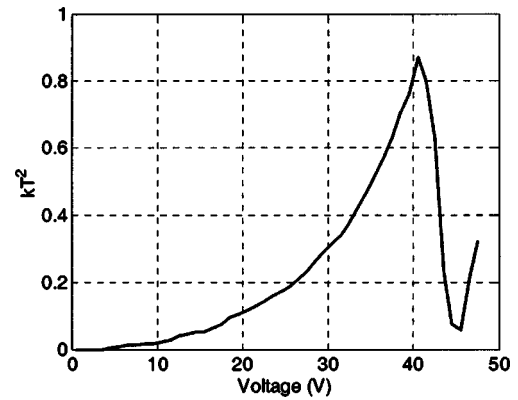


Fig. 13. Electromechanical coupling efficiency of CMUT device as measured from capacitance

able to conclude that the model we used predicted the actual response well. The difference between the height of the peaks of the measured and simulated responses is the result of the structural and electrical losses that are not accounted in the model.

Fig. 12 on the other hand, compares the imaginary part of the electrical input impedance. There is a good match between the measurement and simulation, especially in the antiresonance frequency. Yet, the discrepancy in this case, is the result of the parasitic capacitance that is not accounted in the model, which allows us to measure the parasitic capacitance of the device.

In addition to validating the equivalent model, electrical input impedance measurements also allowed us to measure the electromechanical coupling coefficient  $k_T^2$ , which is extracted from the imaginary part of the input impedance. There are two methods to calculate  $k_T^2$  from the impedance data. One of them depends on the measurement of the resonance and antiresonance frequencies. The other one uses the change in the capacitance as a function of voltage. The details of these calculations were given in the section, “Electromechanical Coupling Coefficient” and can also be found in (Kuhl 1954; Fraser and Reynolds 2000). Fig. 13 shows the  $k_T^2$  of the same device as calculated from the measured capacitance versus the voltage curve. The  $k_T^2$  value increases with increasing bias voltage as predicted, and reaches to  $\sim 0.9$  just before collapse which occurs at 41 V. This plot indeed demonstrates that the conversion efficiency from the electrical port to mechani-

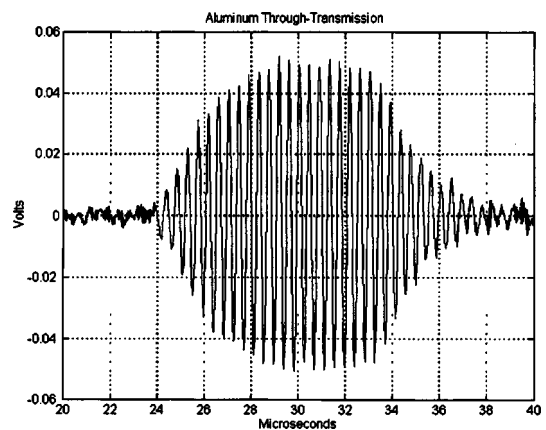


Fig. 14. Through transmission experiment in air through a 3 mm thick aluminum block at 2.3 MHz

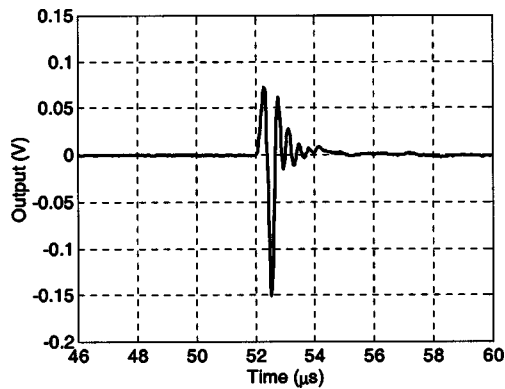


Fig. 15. Pulse-echo measurement in immersion

cal port can be close to unity. This means that CMUTs can be used as efficient acoustical transduction devices.

### Through-Transmission in Air

While showing the electrical input impedance measurements, we demonstrated that CMUT can be used as an efficient acoustical transducer. Fig. 14 shows a through-transmission experiment performed in air using two identical CMUT transducers facing each other in a pitch-catch form. The transducers are biased using the same circuit described earlier. One of them is operated as a transmitter and the other one as a receiver with a front-end amplifier. A 3 mm thick aluminum (Al) block is placed between the transducers to measure the through transmission. The experiment is done at 2.3 MHz with a 20 cycle sinusoidal burst. At this frequency, the total loss in air and in the Al block is calculated to be 87 dB, most of which is due to the impedance mismatch between air and Al. The received signal shown in Fig. 14 has 16 dB of signal-to-noise-ratio. This translates into a dynamic range of 103 dB per 1 V excitation on the transmitter without any matching on the transmitter and receiver transducer.

### Pulse-Echo Measurements in Immersion

For immersion applications, the gap between the membrane and the substrate has to be vacuum sealed. Otherwise, the fluid gets into the cavity in which case the membranes cease to operate. Fig. 15 shows a pulse-echo result obtained from such a device. A thick block of steel is placed in front of the transducer 3.9 cm away. The CMUT transducer is excited with a 20 V, 200 ns pulse at a dc bias voltage of 40 V. The reflection from the steel block is obtained with the same transducer and measured with an oscilloscope. No receiving circuitry was used to switch between transmit and receive and the received signal was not amplified.

Because the acoustical impedance of the immersed medium is much larger than the mechanical impedance of the CMUT, we expect the resonant behavior to be overdamped resulting in a broadband frequency response. By taking the Fourier transform of the pulse response of Fig. 15, it was possible to obtain the frequency response of the CMUT transducer which is shown in Fig. 16. Because it was a pulse-echo measurement, the bandwidth is calculated using the 6-dB points of the frequency response. This particular device showed 123% fractional bandwidth around 1.9 MHz. The benefit of the wide frequency bandwidth in immersion applications is the high-temporal resolution which translates into high-axial resolution. In applications where it is important to de-

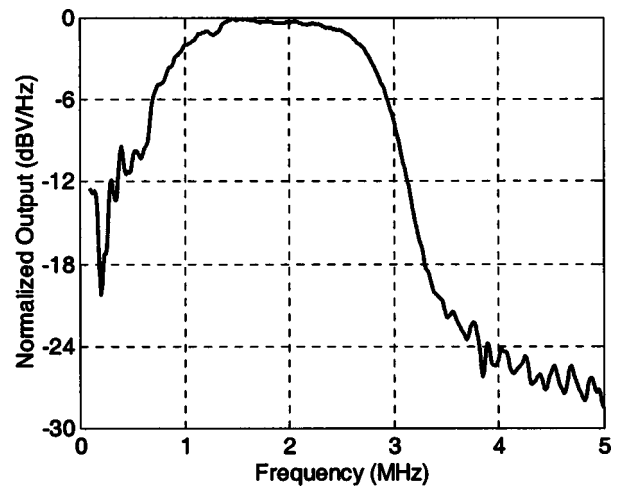


Fig. 16. Frequency response in immersion obtained from pulse-echo response: 6-dB fractional bandwidth is 123%

tect small defects which are close to each other, wide frequency bandwidth allows one to resolve them.

### Applications

The characterization results we showed in the previous section, demonstrate that CMUTs are efficient transduction devices for generation and detection of acoustical signals both in air and water. In immersion applications, the resonant behavior of the CMUT turns into a broadband frequency behavior because of the low-mechanical impedance.

One of the immediate applications of the CMUTs in air, is to use them in through transmission experiments to investigate samples for internal defects. The feasibility of this application was proved with the experiment result shown in Fig. 14. The same experiment setup is used to investigate a 3 mm thick Al block which is intentionally dented. The depth of the dent, which is plus shaped and 3 cm in size, is 500  $\mu\text{m}$ . The transmitting and receiving CMUTs are scanned in space and the through-transmission signals are recorded. Fig. 17 shows the images obtained by plotting the amplitude and the phase of the recorded signals in the scan space. Note that, no image processing is performed, and the dent in the Al block is clearly visible. The arti-

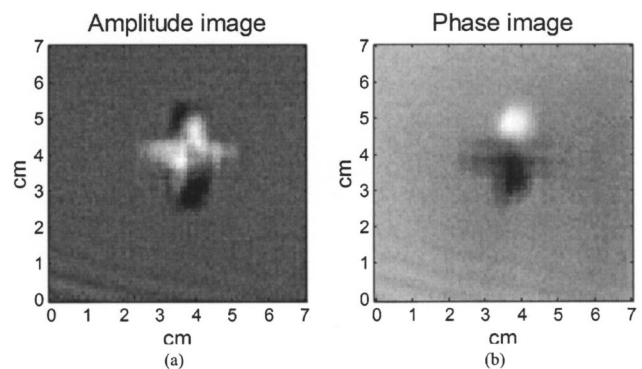
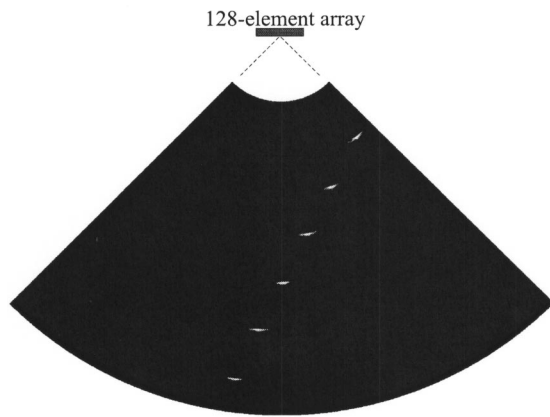


Fig. 17. Image of dented Al block obtained with through-transmission measurements while scanning surface mechanically



**Fig. 18.** Phased array image of 380  $\mu\text{m}$  diameter steel wires inside oil tank using 128 element 1D CMUT array

facts on the lower left corner of both images are believed to be the result of the surface finish of the Al block.

When operated in immersion, CMUTs provide wide bandwidth operation, which opens a whole space of applications. One obvious one is to do the nondestructive testing in immersion. In this way, it is possible to avoid the losses due to the large impedance mismatch between solids and air. In addition, it is possible to achieve high resolution in defect detection.

By virtue of micromachining process, it is possible to fabricate CMUTs into arrays. In array operation, phase delays can be added to each element both in transmit and receive to steer and focus the acoustic beam and to listen to acoustical signals from a certain location in space. This concept has been utilized by medical imaging community extensively for ultrasonic tissue imaging. CMUTs have been shown to perform well in such applications as well (Oralkan et al. 2002). Fig. 18 demonstrates such an example where 380  $\mu\text{m}$  diameter steel wires are imaged in an oil tank by using a 128-element CMUT array. The imaging depth is 21 cm, and the angle of the imaging plane is  $90^\circ$ .

## Conclusion

CMUTs have emerged in the last decade as a means of generating and detecting acoustical signals by using electrostatic principles. It has been shown that CMUTs can operate comparably to their piezoelectric counterparts both in air and immersion. In this paper, we described the basic principles of operation of CMUTs together with measurement results. We showed that we can indeed predict the behavior of CMUTs beforehand, and design for specific targets. We also described the fabrication process in its simplest form which is based on a wet sacrificial release process. Finally, we demonstrated the feasibility of using CMUTs in ultrasound applications by showing some imaging results both in air and immersion.

## Acknowledgments

Research on capacitive micromachined ultrasonic transducers has been funded by DARPA and ONR.

## References

- Bayram, B., Yaralioglu, G. G., and Khuri-Yakub, B. T. (2001). "Influence of the electrode size and location on the performance of a CMUT." *2001 IEEE Int. Ultrasonics Symposium*, Atlanta, October 7–10.
- Belincourt, D. (1971). "Piezoelectric crystals and ceramics." *Ultrasonic transducer materials*, O.E. Mattiat, ed., Plenum, New York.
- Cheng, C. H., Ergun, A. S., and Khuri-Yakub, B. T. (2002). "Electrical through wafer interconnects with 0.05 pico farads parasitic capacitance on 400  $\mu\text{m}$  thick silicon substrate." *Solid State Sensor, Actuator and Microsystems Workshop, Hilton Head Island, S.C.*, June 2–6, 157–160.
- Fraser, J., and Reynolds, P. (2000). "Finite-element method for determination of electromechanical coupling coefficient for piezoelectric and capacitive micromachined ultrasonic transducers." *Joint 140th Meeting of the Acoustical Society of America/Noise Control*, Newport Beach, Calif., December 3–8.
- Haller, M. I., and Khuri-Yakub, B. T. (1996). "A surface micromachined electrostatic ultrasonic air transducer." *IEEE Trans. Ultrason. Ferroelectr. Freq. Control*, 43(1), 1–6.
- Hunt, F. V. (1982). *Electroacoustics; the analysis of transduction, and its historical background*, 2nd Ed., Harvard University Press, Cambridge, Mass.
- Jin, X. C., Ladabaum, I., Degertekin, L., Calmes, S., and Khuri-Yakub, B. T. (1999). "Fabrication and characterization of surface micromachined capacitive ultrasonic transducers." *J. Microelectromech. Syst.*, 8(1), 100–114.
- Kuhl, W., Schodder, G. R., and Schroder, F. K. (1954). "Condenser transmitters and microphones with solid dielectric for airborne ultrasonics." *Acustica*, 4(5), 520.
- Ladabaum, I., Jin, Xuecheng, Soh, H. T., Atalar, A., and Khuri-Yakub, B. T. (1998). "Surface micromachined capacitive ultrasonic transducers." *IEEE Trans. Ultrason. Ferroelectr. Freq. Control*, 45(3), 678–690.
- Mason, W. P. (1948). *Electromechanical transducers and wave filters*, Van Nostrand, London.
- Mastrangelo, and Hsu, C. H. (1993a). "Mechanical stability and adhesion of microstructures under capillary forces. I: Basic theory." *J. Microelectromech. Syst.*, 2(1), 33–43.
- Mastrangelo, and Hsu, C. H. (1993b). "Mechanical stability and adhesion of microstructures under capillary forces. II: Experiments." *J. Microelectromech. Syst.* 2(1), 44–55.
- Oralkan, O., Ergun, A. S., Johnson, J. A., Karaman, M., Demirci, U., Kaviani, K., Lee, T. H., and Khuri-Yakub, B. T. (2002). "Capacitive micromachined ultrasonic transducers: Next generation arrays for acoustic imaging?" *IEEE Trans. Ultrason., Ferroelect., Freq. Control*, 49(11), 1596–1610.
- Soh, H. T., Ladabaum, I., Atalar, A., Quate, C. F., and Khuri-Yakub, B. T. (1996). "Silicon micromachined ultrasonic immersion transducers." *Appl. Phys. Lett.*, 69(24), 3674–3676.